

Reaction dynamics of photochromic dithienylethene derivatives

J. Ern ^a, A.T. Bens ^b, H.-D. Martin ^b, S. Mukamel ^c, D. Schmid ^a, S. Tretiak ^c,
E. Tsiper ^c, C. Kryschi ^{a,*}

^a *Lehrstuhl für Festkörperspektroskopie (IPkM), Heinrich-Heine-Universität, D-40225 Düsseldorf, Germany*

^b *Institut für Organische Chemie und Makromolekulare Chemie I, Heinrich-Heine-Universität, D-40225 Düsseldorf, Germany*

^c *Department of Chemistry, University of Rochester, Rochester, NY 14627, USA*

Received 2 April 1999

Abstract

The reaction dynamics of the photochromic ring-opening reaction of 1,2-bis(5-formyl-2-methyl-thien-3-yl)perfluorocyclopentene (CHO-BMTFP) in dichloromethane solution was investigated using femtosecond transient absorption spectroscopy. The data were analyzed in terms of a model potential and single-electron density matrices, which were calculated using the collective electronic oscillator (CEO) approach and the INDO/S semiempirical Hamiltonian. The S_0 – S_1 and S_0 – S_2 transitions of the closed isomer were resonantly excited using 120 fs pump pulses at 610 and 410 nm, respectively. A temporally delayed white light continuum probe pulse monitors the decay of the S_1 or S_2 state as well as the recovery of the S_0 state. Within the first picosecond after excitation, CHO-BMTFP was observed to undergo a fast structural relaxation along the S_1 potential energy surface into a minimum constituting a precursor of the ring-opening process. The rather long lifetime of the precursor, $\tau_2 = 13$ ps, was consistent with the calculated potential barrier in front of the conical intersection with the S_0 potential energy surface, which may arise from stabilization of the nearly planar closed isomer by an efficiently delocalized π -electron system. © 1999 Elsevier Science B.V. All rights reserved.

Keywords: Photochromism; Dithienylethenes; Reaction kinetics; Femtosecond laser spectroscopy

1. Introduction

Photochromic dithienylethene derivatives have received much attention as potential materials for optical data storage media and optical computer devices [1–6]. The photochromic electrocyclic reaction of this class of photochromic compounds is understood

to obey the Woodward–Hoffmann rules applied to the π molecular orbital symmetries of cyclohexadiene (closed isomer) and hexatriene (open isomer) [7]. Ring opening and ring closure reactions occur photochemically in the conrotatory mode, while the thermally induced ground-state reaction, predicted to take place in the disrotatory mode, is sterically hindered by the two trans-standing methyl groups in the 2' position of the thiophene rings. Fig. 1 shows the absorption spectra of the open isomer (solid line) and closed isomer (dashed line) of 1,2-bis(5-formyl-2-

* Corresponding author. Tel.: +49-211-8114813; fax: +49-211-8114850; e-mail: ckryschi@mail.rz.uni-duesseldorf.de

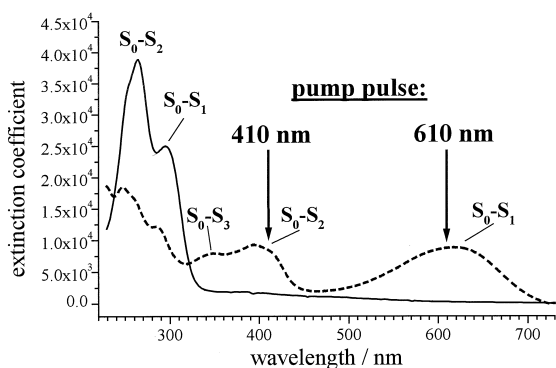


Fig. 1. Absorption spectra of the open (solid line) and closed (dashed line) isomer of CHO-BMTFP in CH_2Cl_2 .

methyl-thien-3-yl)perfluorocyclopentene (CHO-BMTFP). The structure formulae of both isomers are depicted in Fig. 2. The assignment of the absorption bands to the excited singlet states is based on collective electronic oscillator (CEO) calculations of the respective isomers of CHO-BMTFP, geometry-optimized at the AM1 [8] level. Upon UV irradiation, the open isomer undergoes a ring-closure reaction, while the ring-opening reaction may be induced by excitation with visible light. Previous time-resolved studies of electrocyclic reactions in fulgids and other dithienylethene derivatives have shown that both ring-opening and ring-closure processes occur in the ps time domain [9–15]. Until now, reaction kinetics of only four dithienylethene derivatives, namely 1,2-bis(2,4,5-trimethyl-thien-3-yl)maleic anhydride, and three differently substituted 1,2-bis(2-methyl-thien-3-yl)perfluorocyclopentenes, have been investigated on the ps and fs timescale, respectively [12–15]. The ps transient absorption spectroscopy studies of

the maleic anhydride derivative in solution and of 1,2-bis(2-methyl-thien-3-yl)perfluorocyclopentenes in solution as well as in the crystalline phase, lead to an estimation of the time constants of the ring opening and ring closure reaction of shorter than 10 ps [12,14]. Analogous investigations of the open isomer of the oligothiophene derivative of BMTFP, with femtosecond time resolution, yield a ring-closure reaction time constant of about 1.1 ps [13]. Recently, the dynamics of the ring-opening reaction of 1,2-bis(2-methyl-5-(2-(4-benzoyl-phenyl-vinyl))-thien-3-yl)perfluorocyclopentene in solution were investigated with fs transient absorption spectroscopy and biexponential decays of the photoinduced absorption with the time constants, $\tau_L = 1.9$ ps and $\tau_{\text{dis}} = 9$ ps were observed [15].

In the present study, we have investigated the ring-opening reaction kinetics of 1,2-bis(5-formyl-2-methyl-thien-3-yl)perfluorocyclopentene (CHO-BMTFP) in dichloromethane solution with fs transient absorption spectroscopy. CHO-BMTFP was excited to the S_1 and S_2 state using 120 fs pump pulses tuned to the respective maxima of the first and second absorption band (i.e., at 610 and 410 nm, see Fig. 1). The excited state relaxation as well as the recovery of the S_0 state of the closed isomer were monitored by temporally delayed white light probe pulses (350–850 nm). The transients of photoinduced absorption and bleaching were analyzed in terms of a potential model extracted from calculations of the S_0 , S_1 , and S_2 potential energy hyperlines, performed in the recently developed collective electronic oscillator (CEO) approach [16–18]. The theoretical analysis allows the ascribing of the observed decay dynamics to a fast structural relaxation process to a precursor, forming a minimum in the S_1

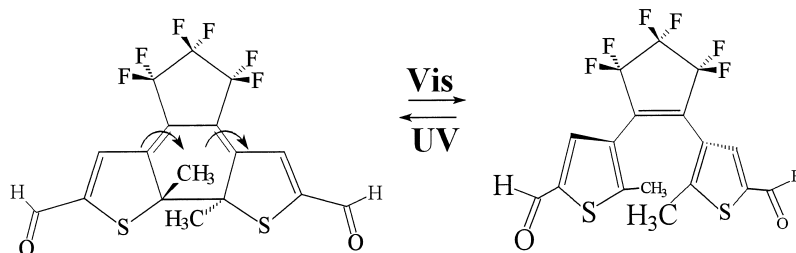


Fig. 2. Structure formulae of the open (left) and closed (right) isomer of CHO-BMTFP.

potential surface, which is separated from the conical intersection by a potential barrier.

2. Experimental

Transient absorption spectra with femtosecond time resolution were measured using the pump-probe technique. Pump and probe pulses were generated by a femtosecond laser system consisting of a passively mode-locked Ti:sapphire laser oscillator (Clark-MXR, NJA-4), a regenerative Ti:sapphire amplifier (Clark-MXR, TRA-1), and an optical parametric amplifier (Clark-MXR, V-GOR). The optical parametric amplifier (OPA) produced, at a repetition rate of 1 kHz, 120 fs pulses with energies of 1–20 μJ , which were tunable between 470 and 670 nm. Either OPA pulses, tuned to 610 nm, or the frequency-doubled amplified oscillator pulses at 410 nm, generated within the OPA, were used as pump pulse beam. The pump pulse intensity was measured with a calibrated powermeter (Coherent, LaserMate Q). The excitation density was varied between 0.5 and 2 mJ/cm^2 . White light continuum probe pulses (300–1000 nm) with a time dispersion of 0.5 ps were generated by focussing the remainder of the fundamental laser pulses (0.2 mJ per pulse), amplified in the OPA, into a 2 mm thick D_2O flow cuvette. A variable delay line provided a temporal delay (τ_D) for the pump pulses of up to 60 ps with a resolution of 2.4 fs. The pump and probe pulses were parallel polarized in all pump-probe experiments. The intensity of the transmitted probe beam with and without pump pulse excitation, $I(p)$ and $I(0)$, respectively, was measured by chopping the pump pulse beam at a frequency of 6 Hz. For each data point, 13 000 pulses were averaged. The ratio of $I(p)/I(0)$ corresponding to the pump pulse induced change of the transmission, $\Delta T = T(p)/T(0)$, was determined with a precision of 10^{-3} . The time dispersion of 0.5 ps over the spectral range of the white light continuum probe pulses was corrected for by determining the $\tau_D = 0$ point from the rise of the bleaching or transient absorption signals at spectral intervals of about 80 cm^{-1} . Transmission spectra of the sample were obtained by dispersing the probe pulses with a polychromator containing a 400 lines/mm grating in combination with a CCD detector system (LOT, InstaSpec IV).

CHO-BMTFP, synthesized and purified as reported by Gilat et al. [5], was dissolved in spectrograde dichloromethane at a concentration of $6.4 \times 10^{-4} \text{ mol/l}$. The solution was pumped at 5 ml/s through a 400 μm flow cell to ensure that, at the 1 kHz repetition rate, a fresh solution volume was probed by every laser pulse.

3. Electronic coherence signatures of ring opening

The ring-opening reaction of CHO-BMTFP was theoretically investigated by calculating the potential energy surfaces of the S_0 , S_1 , and S_2 states along the reaction coordinate q , which is defined as the distance between the two C atoms, C4 and C24 (see Fig. 3), where the bond breaking takes place. Initially, the structures and ground-state (S_0) energies, E_g , of the open and closed isomer were calculated by geometry optimization at the AM1 level followed by single configuration interaction (CI) computations using the semiempirical AM1 procedure of Gaussian 94. The reaction coordinate was modeled by fixing the C4–C24 distance q at values between 430 and 140 pm with a step width of 10 pm. The structures of the intermediate conformations were obtained by optimizing all other geometry parameters at each given q distance, and the associated S_0 energies, $E_g(q)$, were calculated performing single configuration interaction (CI) computations. The resulting S_0 potential energy hyperline $E_g(q)$ is shown in Fig. 4 (open circles). The optimized geometries of the closed and open isomers are localized at $q = 154 \text{ pm}$

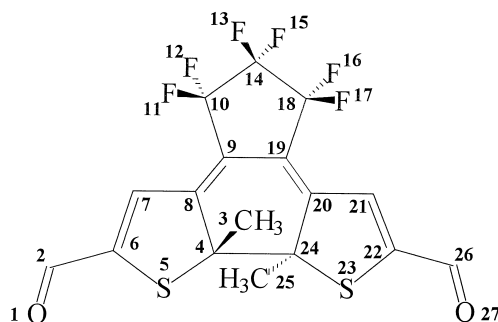


Fig. 3. Structure formula of the closed isomer of CHO-BMTFP with the numbering of the 'heavy' atoms: C, S, F, O.

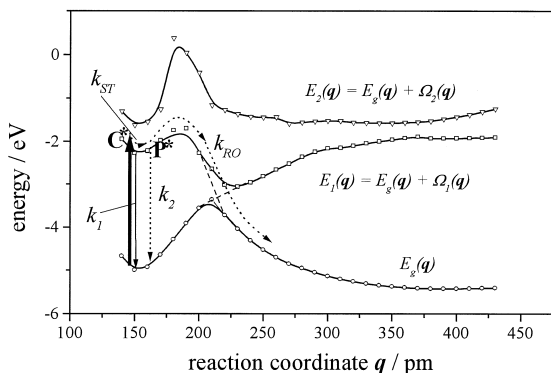


Fig. 4. Schematic illustration of the S_0 , S_1 , and S_2 potential energy surfaces (i.e., $E_g(q)$, $E_1(q)$, $E_2(q)$) along the reaction coordinate q defined as the distance between the atoms C4 and C24 (see Fig. 3); C* and P* denote the initially excited state and precursor, respectively. The rate parameters k_{RO} , k_{ST} , k_1 and k_2 are described in Section 4.

and $q = 393$ pm of the S_0 hyperline and are separated by a large, 1.6 eV potential barrier.

The structural data of the geometry-optimized open and closed isomers as well as those of the intermediate conformations were used as input data for the ZINDO code [19] to compute the INDO/S

Hamiltonian parameters and reduced single-electron density matrices for the S_0 state, $\bar{\rho}_{mn}$:

$$\bar{\rho}_{mn} \equiv \langle g | c_m^+ c_n | g \rangle, \quad (1)$$

where c_m^+ (c_m) are creation (annihilation) operators of an electron at the m th atomic orbital, and $|g\rangle$ is the ground-state multi-electron wave function. The diagonal elements $\bar{\rho}_{nn}$ represent the electronic charge density at the n th orbital, whereas the off-diagonal elements $\bar{\rho}_{mn}$, with $m \neq n$, describe the bond-order (electronic coherence) structure associated with a pair of atomic orbitals. The ground-state density matrix $\bar{\rho}_{mn}$ is expanded using only the $2p_x$ atomic orbitals of the heavy atoms (i.e., C, O, S and F), which form the π -electron system and therefore constitute the HOMO and LUMO. The resulting $k \times k$ matrices (where $k = 27$ is the number of heavy atoms) are displayed as contour plots (ξ_0 in Fig. 5). The labeling of atoms is given in Fig. 3. The top panels in Fig. 5 show the ground-state density matrices for the closed isomer ($q = 154$ pm) and for the open isomer ($q = 393$ pm). The differences in the π -electron conjugation are clearly reflected in the off-diagonal elements: while the π -electron system

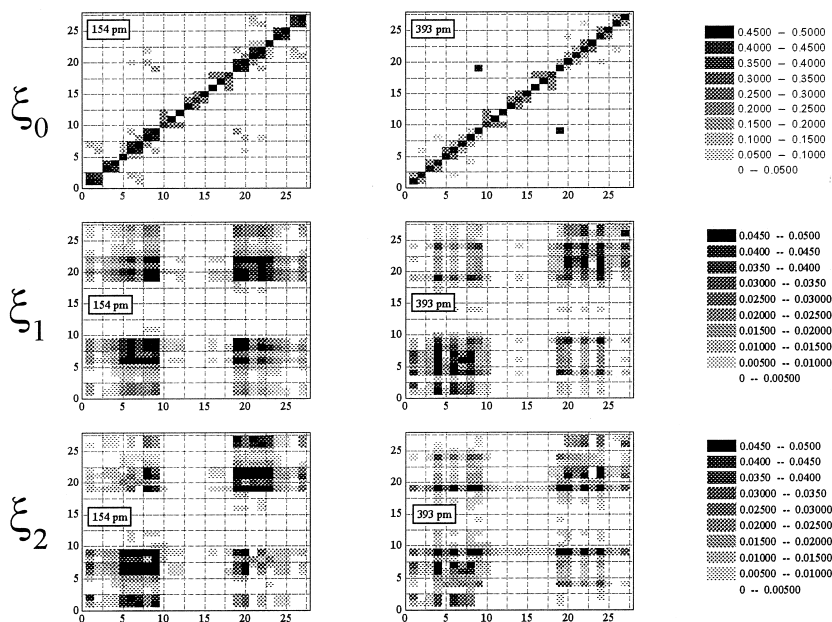


Fig. 5. 2D-Contour plots of the electron modes of the closed isomer: ξ_0 , ξ_1 , ξ_2 (left side) and of the open isomer: ξ'_0 , ξ'_1 , ξ'_2 (right side).

of the closed isomer is delocalized along the π -conjugated backbone (O1–C2–C6–C7–C8–C9–C19–C20–C21–C22–C26–O27) over the dithienylethene unit, for the open isomer the π -conjugation is less pronounced. In particular, the off-diagonal 9/19 and 19/9 matrix elements experience the largest differences in the course of the electrocyclic reaction: they are very small for the closed isomer and substantially increase with rising q . The dependence of $\rho_{9,19}$ on q exhibits a sharp rise between 175 and 225 pm (see Fig. 6).

We employed the CEO technique [16–18] to compute and analyze the optical spectra using as $\bar{\rho}$ an input. The molecular transition dipole is a single-electron operator which may be expanded in the form $P = \sum_{mn} \mu_{mn} c_m^+ c_n$, where μ_{mn} is the transition dipole moment matrix element. The optical transitions between the ground state, g , and excited states, ν , are described using the transition density matrix elements:

$$(\xi_\nu)_{mn} = \langle \nu | c_m^+ c_n | g \rangle. \quad (2)$$

The linear optical response is given by the frequency-dependent linear polarizability $\alpha(\omega)$:

$$\alpha(\omega) = \sum_\nu \sum_{mkl} \mu_{mn} \mu_{kl} \frac{2\Omega_\nu (\xi_\nu)_{mn} (\xi_\nu)_{kl}}{\Omega_\nu^2 - (\omega + i\Gamma_\nu)^2}. \quad (3)$$

Here Γ_ν is the dephasing rate, and ν is the index of the excited singlet states, $|\nu\rangle$ with energies, E_ν , and

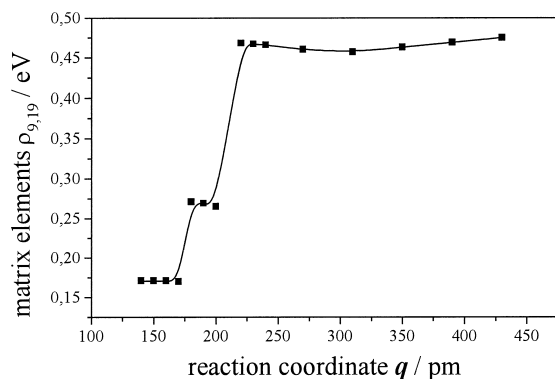


Fig. 6. Variation of the ground-state density matrix element between the atoms C9 and C19 ($\rho_{9,19}$) along the reaction coordinate q ; the value of $\rho_{9,19}$, which reflects the π conjugation between the blocks L and R of CHO-BMTEP, increases sharply as q increases from 175 to 225 pm. This characterizes the change of the single to double bond (see Fig. 2).

transition frequencies, $\Omega_\nu = E_\nu - E_g$. The matrices, ξ_ν , and frequencies, Ω_ν , are determined by solving the time dependent Hatree–Fock (TDHF) equations for the density matrix

$$\begin{aligned} \rho_{mn}(t) &\equiv \langle \Psi(t) | c_m^+ c_n | \Psi(t) \rangle \\ &= \bar{\rho}_{mn} + \sum_\nu a_\nu(t) (\xi_\nu)_{mn} + a_\nu^*(t) (\xi_\nu^+)_{mn}, \end{aligned} \quad (4)$$

where $\Psi(t)$ represents the multi-electron wave function of the molecule driven by the external electromagnetic field. The equations were solved using the Density Matrix Spectral-Moment Algorithm (DSMA) [18]. This procedure yields the matrices, ξ_ν , and frequencies, Ω_ν , computed as eigenfunctions and eigenvalues of the linearized TDHF equation, respectively. The adiabatic potential energy surfaces of the excited states, S_1 and S_2 , along the reaction coordinate q can be computed by adding the energy of the electronic mode, $\Omega_\nu(q)$ with $\nu = 1, 2$ to the S_0 energy at the desired nuclear configuration q [20,21]

$$E_\nu(q) = E_g(q) + \Omega_\nu(q). \quad (5)$$

The S_1 and S_2 potential energy hyperlines, $E_1(q)$ and $E_2(q)$, calculated as functions of q (\equiv C4–C24 distance), are shown in Fig. 4 (see open squares and open triangles). Since the electronic modes were obtained in the adiabatic approximation, the resulting S_1 and S_2 hyperlines do not lead to reliable information in the region of the photochemical reaction funnel. Pericyclic singlet reactions are predicted to occur nonadiabatically via a conical intersection to the S_0 potential energy surface [22–24]. We assumed that the potential barrier at $q = 180$ pm on the calculated S_1 hyperline is followed by a conical intersection point at $q \approx 215$ pm, as indicated by the dashed crossed connection lines between the S_0 and S_1 hyperlines.

ξ constitute electronic normal modes, since they describe collective (oscillatory) motions of holes and electrons (e.g., the oscillating excitation density). Examination of these modes allows for the interpretation of optical spectra in terms of charge distributions in excited states and motions of electrons and holes in real space, totally avoiding the time-consuming calculation of multi-electron eigenstates [16–18]. While the diagonal elements, $(\xi_\nu)_{nn}$, represent the

photoinduced net charge on the n th atomic orbital, the dynamical bond-order (or coherences) between the n th and m th two atomic orbital is represented by the off-diagonal elements, $(\xi_\nu)_{nm}$ ($n \neq m$). Performing this procedure for CHO-BMTPF, we calculated the two lowest-energy electronic modes, ξ_ν ($\nu = 1, 2$), with eigenfrequencies corresponding to the excitation energies of the S_ν states. The ν th oscillator describes the optical transition between the ground state and the ν th excited state. The contour plots of the first electronic modes, ξ_1 (closed isomer) and ξ'_1 (open isomer), depicted in Fig. 5 (center), directly illustrate both photoinduced net charges and photoinduced electron-hole pairs (i.e., coherences) for the transition to the reactive S_1 state. Both electronic modes are almost symmetric with respect to the diagonal ($\xi_{mn} \approx \xi_{nm}$) as well as to the anti-diagonal ($m-n$) direction. The variation along the diagonal exhibits the center of the electron-hole motion, whereas its delocalization is reflected by the off-diagonal elements. In the case of ξ_1 (closed isomer), the optical excitation is delocalized along the C6–C7–C8–C9–C19–C20–C21–C22 chain. As the contour plot of ξ'_1 (open isomer) shows, ring opening is accompanied by an interruption of the delocalization between C9 and C19. The contour plots of the second electronic modes, ξ_2 (closed isomer) and ξ'_2 (open isomer) (see Fig. 5, bottom), display similar features. However, the size of the largest exciton coherence (from C6 to C22) of ξ_2 is somewhat smaller and the delocalization is less pronounced. The electronic excitation, ξ'_2 , shows relevant coherences only along C8–C9–C19–C20, C4–C6–C7 and C24–C22–C21.

As suggested by the structure of the contour plots of ξ_1 and ξ_2 (see Fig. 5), CHO-BMTPF can be divided into three atom groups ('blocks') L (left), R (right), and C (central) corresponding to the heavy-atom chains between O1–C9, C19–O27 and C10–C18, respectively. Block C acts as a separator and is approximately independent of q . In contrast, variations of q significantly affect the coherences within and between the L and R blocks (see the diagonal and off-diagonal rectangles in Fig. 5). To elucidate this feature in more detail, we defined a 2×2 density matrix coarse grained over the L and R blocks of ξ . ξ_{LL} (ξ_{RR}) is computed by summing the absolute values of the elements within the L (R) block. Simi-

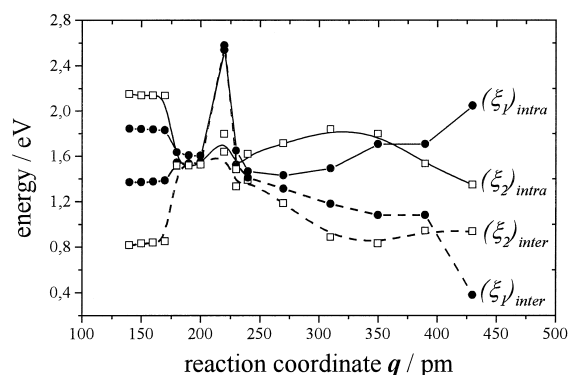


Fig. 7. Variations of the total electronic coherences within (solid lines, ξ_{intra}) and between (dashed lines, ξ_{inter}) the blocks L (O1–C9) and R (C19–O27) along the reaction coordinate q for the S_1 and S_2 states. The coherences were calculated by summation of the absolute values of the respective matrix elements in the contour plots of ξ_1 and ξ_2 displayed in Fig. 4 as explained in the text.

larly ξ_{LR} and ξ_{RL} are obtained by summing the absolute values of off-diagonal elements between the blocks. The global *intra*block (*inter*block) coherence is given by the sum $\xi_{\text{intra}} = \xi_{LL} + \xi_{RR}$ ($\xi_{\text{inter}} = \xi_{LR} + \xi_{RL}$). The variation of the global coherences along the S_1 hyperline are displayed in Fig. 7. The plot clearly shows that $(\xi_1)_{\text{inter}}$ decreases while $(\xi_1)_{\text{intra}}$ increases in the course of the ring opening reaction. The global coherences for the ξ_2 mode are also depicted in Fig. 7. In this case, the $(\xi_2)_{\text{inter}}$ and $(\xi_2)_{\text{intra}}$ coherences merge as q is increased.

4. Transient absorption spectra

To probe the differences in the reactivity of the S_1 and S_2 states of closed CHO-BMTPF in dichloromethane solution, transient absorption spectra were recorded with pump pulses tuned to the S_0 – S_1 transition at 610 nm and to the S_0 – S_2 transition at 410 nm, as indicated by arrows in Fig. 2. The time dependence of the photoinduced transmission changes $\Delta T(\tau_D, \lambda)$ is given by the delay time τ_D of the pump relatively to the arrival time (i.e., $\tau_D = 0$) of the probe in the sample. The temporal evolutions of the transient absorption spectra between -0.5 ps and $+31$ ps for 610 nm and between -0.6 ps and $+61$ ps for 410 nm are shown in Figs. 8 and 9,

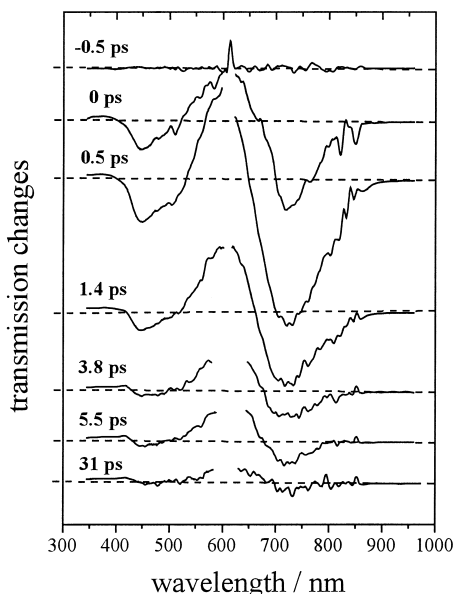
transient absorption spectra excited at 610 nm

Fig. 8. Temporal evolution of the transient absorption spectra recorded at delay times τ_D between -0.5 ps and $+31$ ps. The excitation wavelength is 610 nm.

respectively. The spectra at $\tau_D \leq -0.5$ ps provide the baseline with $\Delta T(\lambda) \approx 1$. The peaks at 610 nm and 410 nm are due to scattered light of the pump pulses. While transmission changes with $\Delta T(\lambda) > 1$ characterize photoinduced bleaching of the S_0 - S_1 and S_0 - S_2 spectra at 520–680 nm and 360–430 nm, respectively, the photoinduced (S_1 - S_n) absorption, appearing in the wavelength ranges 430–520 nm and 680–850 nm, is ascribed to transmission changes with $\Delta T(\tau) < 1$. The time dependence of the photoinduced transmission changes recorded at a fixed wavelength $\lambda = \lambda_0$ (i.e., $\Delta T(\tau_D)$) is denoted as transient or decay curve of photoinduced bleaching ($\Delta T(\tau_D) > 1$) or absorption ($\Delta T(\tau_D) < 1$). We investigated the influence of the pump pulse intensity on the transients and did not observe any significant difference in the decay dynamics for excitation densities between 0.5 and 2 mJ/cm².

Figs. 10 and 11 depict photoinduced bleaching (middle panels) and absorption (top and bottom panels) transients, as examples for the respective wavelength range, which were measured upon excitation of the S_0 - S_1 transition at 610 nm (see Fig. 10) and

the S_0 - S_2 transition at 410 nm (see Fig. 11). The photoinduced bleaching transients (see Figs. 10 and 11, at center: $\lambda_{\text{det}} = 544$ nm or $\lambda_{\text{det}} = 581$ nm, solid line), displaying the recovery dynamics of the S_0 state of the closed isomer, can be described by the exponential decay function $A_0 \times \exp(-\tau_D/\tau_{\text{tb}})$ with the time constant $\tau_{\text{tb}} = 13 \pm 1$ ps. This suggests that the S_0 state is uniformly repopulated by deactivation of a metastable state forming a sufficiently deep minimum in the S_1 potential energy surface. An unstable precursor acting as barrierless exit to a conical intersection with the S_0 potential energy surface is expected to decay within one vibrational period (< 1 ps) to the S_0 state of either the closed and open isomer. This is obviously in contradiction with the observed time constant of the photoinduced bleaching transients of $\tau_{\text{tb}} = 13 \pm 1$ ps. Since CHO-BMTFP is a nonfluorescing compound, the S_0 state of the closed isomer should be repopulated on the ps scale essentially by internal conversion (IC). The two bleaching transients in Figs. 10 and 11 have identical decay dynamics. Within the 50 ps time scale, the signal does not decay to zero. The long-lived bleach-

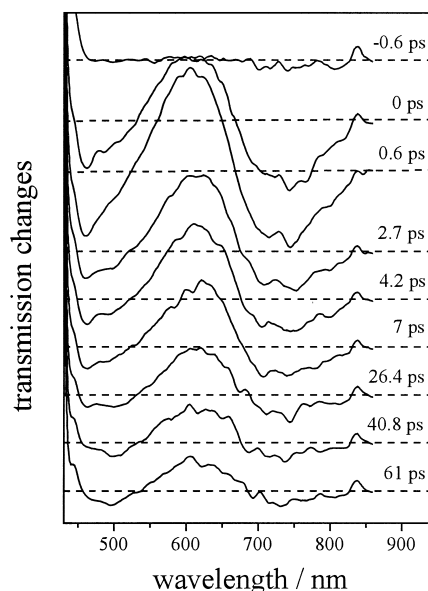
transient absorption spectra excited at 410 nm

Fig. 9. Temporal evolution of the transient absorption spectra recorded at delay times τ_D between -0.6 ps and $+61$ ps. The excitation wavelength is 410 nm.

ing signal, attributed to the population of the triplet state, is somewhat larger for 420 nm excitation (25%) than for 610 nm excitation (20%). The photoinduced absorption transients (see Figs. 10 and 11, bottom and top, solid lines) are very well fitted by a sum of two exponentials: $\Delta T(\tau_D) = A_1 \times (1 -$

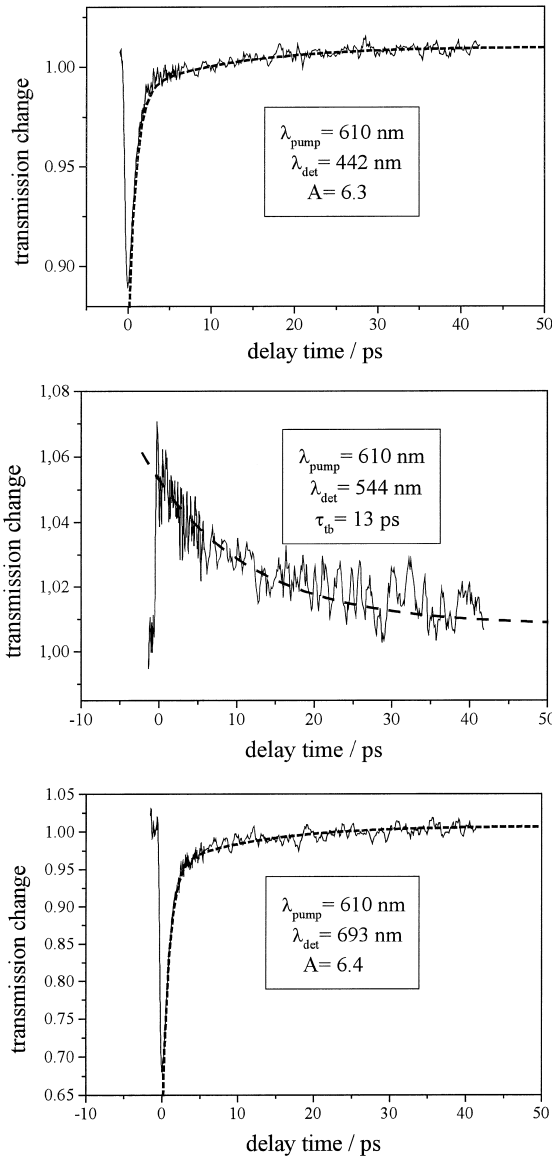


Fig. 10. Transients of photoinduced absorption detected at 442 nm (top), 693 nm (bottom) and transient of photoinduced bleaching detected at 544 nm (center). The pump pulse wavelength is 610 nm.

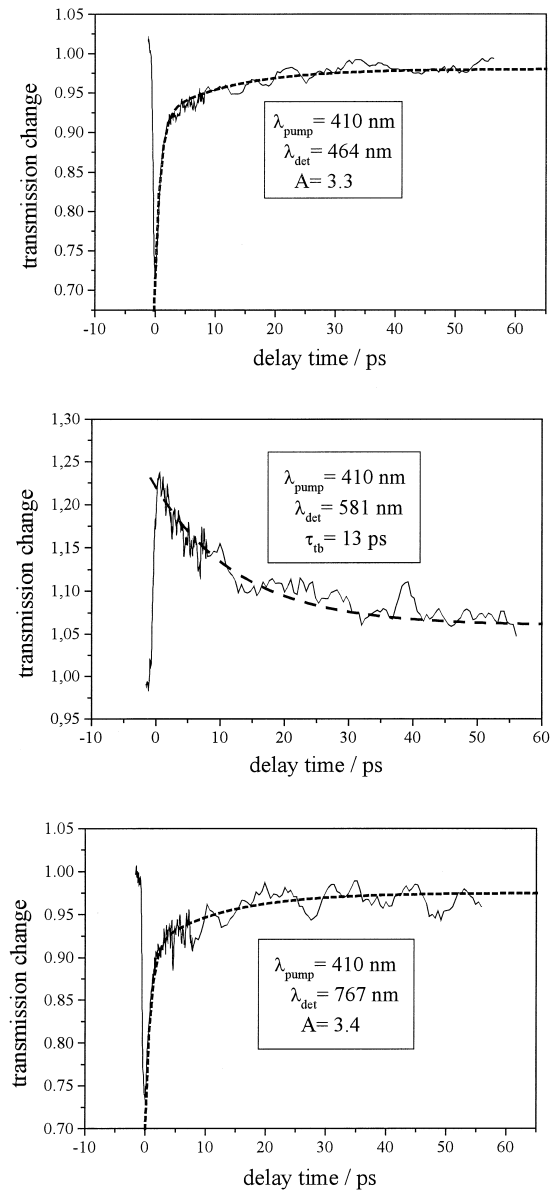


Fig. 11. Transients of photoinduced absorption detected at 464 nm (top), 767 nm (bottom) and transient of photoinduced bleaching detected at 581 nm (center). The pump pulse wavelength is 410 nm.

$\exp(-\tau_D/\tau_1)) + A_2 \times (1 - \exp(-\tau_D/\tau_2))$ (thick broken lines) with the time constants $\tau_1 = 0.9$ ps and $\tau_2 = 13$ ps. The fit of the transients excited at 610 nm (S_0 - S_1 absorption) has an amplitude ratio of $A = A_1/A_2 = 6.1 \pm 0.3$, while that for the transients

excited at 410 nm (S_0 – S_2 absorption) is about 3.3. To understand the reaction kinetics causing these decay characteristics, the absorption transients are analyzed in terms of a two-term sequential reaction model which is derived in the following way.

We ascribe the short time dynamics ($\tau_1 = 0.9$ ps) to fast structural relaxation of the initially prepared state C^* on the S_1 potential energy surface, which decays to a metastable state P^* forming a minimum in the S_1 potential energy surface (see Fig. 4). The existence of this state, P^* , is justified by the rather small quantum yield (4%) of the ring-opening reaction induced at 610 nm [25] and by the slow recovery of the S_0 state with a time constant of about 13 ps. P^* , the precursor of the reaction, is separated by a barrier from a (weakly) avoided crossing or conical interaction between the S_0 and S_1 surfaces, where the photochemical reaction takes place. The decay rate of the initially excited state C^* , $k_1 = 1/\tau_1$, is determined by the rate constant of conformational relaxation to the precursor P^* , k_{ST} , and that of all photophysical unimolecular decay processes back to the S_0 state of the closed isomer: $k_1 = k^C + k_{ST}$, where $k^C = k_{IC}^C + k_{ISC}^C + k_F^C$, is the sum of the rate constants of internal conversion (IC), intersystem crossing (ISC) and intrinsic fluorescence (F), respectively. The population density of the precursor, $[P^*]$, decays by the ring-opening reaction (k_{RO}), as well as by radiative and radiationless deactivation to the S_0 state of the closed isomer: $k_2 = k_{RO} + k^P$ with $k^P = k_{IC}^P + k_{ISC}^P + k_F^P$. The reaction kinetics at $t = \tau_D > 300$ fs (i.e., after pump pulse excitation) can be approximated by the rate equations describing the temporal evolutions of the population densities $[S_0]$, $[C^*(t)]$, and $[P^*(t)]$ of the ground state, S_0 , the initially excited state, C^* , and the subsequently populated (structurally relaxed) precursor, P^* , respectively:

$$\frac{d[C^*(t)]}{dt} = -k_1[C^*(t)], \quad (6)$$

$$\frac{d[P^*(t)]}{dt} = +k_{ST}[C^*(t)] - k_2[P^*(t)], \quad (7)$$

$$\frac{d[S_0^*(t)]}{dt} = +k^C[C^*(t)] + k^P[P^*(t)], \quad (8)$$

with the boundary conditions $[P^*(t=0)] = [P^*(t=\infty)] = 0$ integration of the coupled differential equations yields:

$$[C^*(t)] = [C_0^*]e^{-k_1t}, \quad (9)$$

$$[P^*(t)] = [C_0^*] \frac{k_{ST}}{k_1 - k_2} (e^{-k_2t} - e^{-k_1t}), \quad (10)$$

$$[S_0(t)] = [S_0(0)] + [C_0^*] \left(\left(k^C - \frac{k^P k_{ST}}{k_1 - k_2} \right) \times \frac{(1 - e^{-k_1t})}{k_1} + \frac{k^P k_{ST}}{k_1 - k_2} \frac{(1 - e^{-k_2t})}{k_2} \right), \quad (11)$$

where $[C_0^*]$ is the population density at $t = 0$. Note that by definition, the total population density $[S_0(t < 0)] = [S_0(0)] + [C_0^*] = 1$. The quantum yield of the ring-opening reaction, Φ_{RO} , is given by the expression:

$$\Phi_{RO} = 1 - \frac{[S_0(\infty)S_0(0)]}{[C_0^*]} = \frac{k_{ST}k_{RO}}{k_1k_2}. \quad (12)$$

In the spectral range of the observed photoinduced absorption, the transmission changes of the white light probe pulse are caused by the states C^* and P^* , and the temporal evolution of ΔT has a biexponential form:

$$1 - \Delta T(t) \propto \left((\alpha_1 - \alpha_0)e^{-k_1t} + (\alpha_2 - \alpha_0) \frac{k_{ST}}{k_1 - k_2} (e^{-k_2t} - e^{-k_1t}) \right) = \left(\left((\alpha_1(\lambda) - \alpha_0(\lambda)) - (\alpha_2(\lambda) - \alpha_0(\lambda)) \frac{k_{ST}}{k_1 k_2} \right) e^{k_1t} + (\alpha_2(\lambda) - \alpha_0(\lambda)) \frac{k_{ST}}{k_1 - k_2} e^{-k_2t} \right), \quad (13)$$

where $\alpha_0(\lambda)$, $\alpha_1(\lambda)$, and $\alpha_2(\lambda)$, are the absorption coefficients of S_0 , C^* , and P^* , respectively. The time constants $\tau_1 = 0.9$ ps and $\tau_2 = 13$ ps and thereby the rate constants $k_1 = 1.1 \times 10^{12} \text{ s}^{-1}$ and $k_2 = 7.7 \times 10^{10} \text{ s}^{-1}$ were obtained from the biexponential fits of the transients in Figs. 10 and 11. To evaluate the rate constant of the ring opening reaction, k_{RO} ,

we used the experimental value of $\Phi_{\text{RO}} \approx 4\%$ [25] and assumed that the structural relaxation to P^* dominated the decay of C^* . This latter assumption is consistent with the fact that the recovery of S_0 does not contain a measurable contribution of a fast component with a time constant of τ_1 . We obtained $k_{\text{RO}} \approx 3.1 \times 10^9 \text{ s}^{-1}$ ($\tau_{\text{RO}} = 325 \text{ ps}$). Since the factor $(k_{\text{ST}})/(k_1 - k_2)$ in Eq. (13) is close to unity, the amplitude ratio $A = A_1/A_2$, obtained from the biexponential fits of the absorption transients, corresponds to $(\alpha_1(\lambda) - \alpha_2(\lambda))/(\alpha_2(\lambda) - \alpha_0(\lambda))$ and reflects thereby the difference in the S_1 – S_n absorption coefficients of the initially excited state C^* and the precursor P^* . $A \approx 6$ in the case of initial excitation of the S_0 – S_1 absorption, and $A \approx 3$ for excitation at 410 nm (S_0 – S_2 absorption), showing that the difference of absorption coefficients $\{\alpha_1(\lambda) - \alpha_2(\lambda)\}$ decreases by a factor of two by going to the shorter wavelength.

5. Conclusions

The combination of forefront experimental and theoretical techniques, femtosecond transient absorption spectroscopy and the collective electronic modes (CEO) approach has made it possible to elucidate the kinetics of the ring-opening reaction of 1,2-bis(5-formyl-2-methyl-thien-3-yl)perfluorocyclopentene (CHO-BMTEP). The determination of the S_0 , S_1 , and S_2 potential energy surfaces along the reaction coordinate q , computed using the semiempirical AM1 procedure and the CEO approach, provides a microscopic model for the analysis of the spectroscopic data. The transient photoinduced absorption and bleaching, monitored at detection wavelengths between 450 and 850 nm, probes structural relaxation dynamics along the S_1 potential energy surface with subsequent decay to the S_0 surface of the closed and open isomer as well as the recovery dynamics of the S_0 state. The theoretical analysis of the absorption transients in terms of the potential model provides the following scenario of excited state dynamics: the 120 fs pump pulse prepares on the S_1 potential energy surface the initially excited state C^* which decays by fast structural relaxation ($\tau_{\text{ST}} \approx 1 \text{ ps}$) to the precursor P^* . Since P^* forms a minimum in the S_1 potential surface, which is separated from the

conical intersection (at $q \approx 215 \text{ pm}$) by a potential barrier (at $q = 180 \text{ pm}$), its lifetime ($\tau_2 \approx 13 \text{ ps}$) is determined by radiationless deactivation to the S_0 state of the closed isomer, whereas the time constant of the ring opening reaction is rather long $\tau_{\text{RO}} \approx 325 \text{ ps}$. The potential barrier presumably arises from stabilization of the closed isomer structure with $q = 180 \text{ pm}$ by maximum delocalization of the π -electron system.

Acknowledgements

This research has been supported by the Volkswagenstiftung (PHOTONIK, Az.: I/71 939) and by the National Science Foundation (Grants No. CHE-9526125). We are grateful to Peter Trommsdorff and Vladimir Chernyak for fruitful discussions.

References

- [1] M. Irie, *Jpn. J. Appl. Phys.* 28 (1989) 215.
- [2] K. Uchida, Y. Nakayama, M. Irie, *Bull. Chem. Soc. Jpn.* 63 (1990) 1311.
- [3] M. Irie, K. Uchida, *Bull. Chem. Soc. Jpn.* 71 (1998) 985.
- [4] S.L. Gilat, S.H. Kawai, J.-M. Lehn, *J. Chem. Soc., Chem. Commun.* (1993) 1439.
- [5] S.L. Gilat, S.H. Kawai, J.-M. Lehn, *Chem. Eur. J.* 1 (1995) 275–284.
- [6] G.M. Tsivgoulis, J.-M. Lehn, *Angew. Chem.* 107 (1995) 1188.
- [7] R.B. Woodward, R. Hoffmann, *The Conservation of Orbital Symmetry*, Verlag Chemie, Weinheim, 1970.
- [8] M.J.S. Dewar, E.G. Zebisch, E.F. Healy, J.J.P. Stewart, *J. Am. Chem. Soc.* 107 (1985) 3902.
- [9] T. Minami, N. Tamai, T. Yamazaki, I. Yamazaki, *J. Phys. Chem.* 95 (1991) 3988.
- [10] M. Handschuh, M. Seibold, H. Port, H.C. Wolf, *J. Phys. Chem. A* 101 (1997) 502.
- [11] N. Tamai, H. Masuhara, *Chem. Phys. Lett.* 27 (1992) 189.
- [12] H. Miyasaka, S. Araki, A. Tabata, T. Nobuto, N. Mataga, M. Irie, *Chem. Phys. Lett.* 230 (1994) 249.
- [13] N. Tamai, T. Saika, T. Shimidzu, M. Irie, *J. Phys. Chem.* 100 (1996) 4689.
- [14] H. Miyasaki, T. Nobuto, A. Itaya, N. Tamai, Masahiro, *Chem. Phys. Lett.* 269 (1997) 281.
- [15] J. Ern, A.T. Bens, A. Bock, H.-D. Martin, C. Kryschi, *J. Lumin.* 76–77 (1998) 90.
- [16] S. Tretiak, V. Cherniak, S. Mukamel, *J. Am. Chem. Soc.* 119 (1997) 11408.

- [17] S. Mukamel, S. Tretiak, Th. Wagersreiter, V. Chernyak, *Science* 277 (1997) 781.
- [18] V. Chernyak, S. Mukamel, *J. Chem. Phys.* 104 (1996) 444.
- [19] M.C. Zerner, G.H. Loew, R.F. Kirchner, U.T. Mueller-Westhoff, *J. Am. Chem. Soc.* 102 (1980) 589.
- [20] E.V. Tsiper, V. Chernyak, S. Tretiak, S. Mukamel, Ground-state-density-matrix algorithm for excited state adiabatic surfaces; application to polyenes, *Chem. Phys. Lett.*, in press.
- [21] E.V. Tsiper, V. Chernyak, S. Tretiak, S. Mukamel, Density matrix spectroscopic algorithm for excited state adiabatic surfaces and molecular dynamics of a protonated schiff base, *J. Chem. Phys.*, in press.
- [22] M. Klessinger, *Pure Appl. Chem.* 69 (1997) 773.
- [23] P. Celani, S. Ottani, M. Olivucci, F. Bernardi, M.A. Robb, *J. Am. Chem. Soc.* 116 (1994) 10141.
- [24] J. Michl, V. Bonacic-Koutecky, *Electronic Aspects of Organic Photochemistry*, Wiley, New York, 1990.
- [25] K. Tsyganenko, PhD thesis, Universite Joseph-Fourier Grenoble I, 1998.